Multi-scale modelling of heat transfer in polyurethane foams

Pavel Ferkl [a], Miloš Toulec [a], Erik Laurini [b], Sabrina Pricl [b], Maurizio Fermeglia [b], Stefan Auffarth [c], Berend Eling [c], Volker Settels [d], Juraj Kosek [a,*]

[a] Department of Chemical Engineering, University of Chemistry and Technology, Prague, Czech Republic
[b] Molecular Simulation Engineering (MOSE) Laboratory, University of Trieste, DIA, Piazzale Europa 1, 34127 Trieste, Italy
[c] BASF Polyurethanes GmbH, Elastogranstr. 60, Lemförde, Germany
[d] BASF SE, Ludwigshafen, Germany

HIGHLIGHTS

- Model for the prediction of heat insulation properties of PU foams is presented.
- Absorption spectrum of PU is computed by quantum chemical density functional theory.
- Thermal conductivity of PU, gas and gas mixtures is calculated by molecular dynamics.
- Equivalent conductivity of foam is determined by homogeneous phase approach.
- Validation by experimental data showed the successfulness of proposed model.

GRAPHICAL ABSTRACT

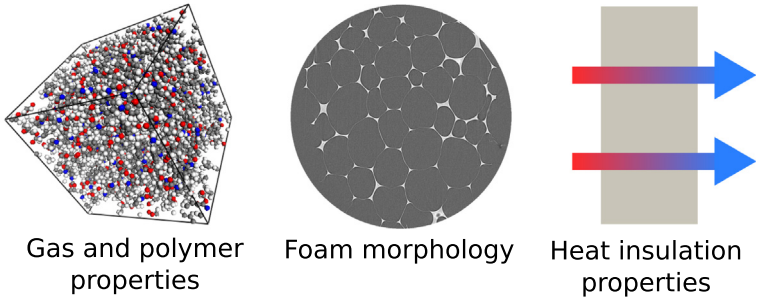

ARTICLE INFO

Accepted 20 June 2017

Keywords:
Foams
Polyurethane
Heat insulation
Thermal conductivity
Radiative heat transfer
Molecular dynamics

ABSTRACT

The influence of morphology and cell gas composition on heat insulation properties of polyurethane (PU) foams was investigated using a multi-scale mathematical model. The polymer absorption coefficient was determined from quantum chemical computations. Reverse non-equilibrium molecular dynamics was used to calculate the thermal conductivity of polymer and gas mixtures relevant to PU foams. The equivalent foam conductivity was calculated using homogeneous phase approach. The individual models were coupled together using suitable surrogate models within MoDeNa framework. To validate the proposed model 9 foam samples were prepared using different recipes, their morphology was characterized and their thermal conductivity was measured. The difference between experimental and predicted values was comparable to experimental error. Developed multi-scale model was used to identify the most suitable relation for the calculation of thermal conductivity of gas mixtures in PU foams and to quantify the influence of foam density, cell size, and strut content on heat insulation properties of PU foams.

1. Introduction

The insulation properties of PU foams are derived from their morphology, i.e., porosity, cell size, strut content, etc., and from the material properties of the polyurethane and the cell gases, i.e., their thermal conductivities and the complex index of refraction of the polymer. Conduction and radiation are the primary modes of heat transfer, because the cells of PU foams are too small for the onset of free convection (Mills, 2007; Klempner et al., 2004). In this work, we employed quantum chemical density functional theory and molecular dynamics simulations to predict material properties of gas and polymer phases.

* Corresponding author.
E-mail address: Juraj.Kosek@vscht.cz (J. Kosek).

Nomenclature

Subscripts

C	cold slab
c	cell
f	foam
g	gas
H	hot slab
p	polymer
s	strut
w	wall

Greek letters

β	extinction coefficient (m^{-1})
κ	absorption coefficient (m^{-1})
λ	wavelength (m)
ν	wavenumber (cm^{-1})
ω	frequency (s^{-1})
ρ	density ($kg\,m^{-3}$)
ε	porosity

Latin letters

$\mathbf{q}$	heat flux ($W\,m^{-2}$)
$\mathbf{v}$	velocity (ms^{-1})
A	surface (m^2)
A_{ij}	Wassiljewa coefficients
c_p	specific heat capacity ($J\,kg^{-1}\,K^{-1}$)
$E_{b\lambda}$	spectral blackbody emissive power ($W\,m^{-3}$)
E_b	blackbody emissive power ($W\,m^{-2}$)
f_s	strut content
G	incident radiation ($W\,m^{-2}$)
G_λ	spectral incident radiation ($W\,m^{-3}$)
k	thermal conductivity ($W\,m^{-1}\,K^{-1}$)
L	domain size (m)
M	molar mass ($kg\,mol^{-1}$)
m	mass (kg)
R	gas constant ($J\,mol^{-1}\,K^{-1}$)
S	Sutherland constant (K)
T	temperature (K)
t	time (s)
V	volume (m^3)
y	molar fraction

We take special care in predicting the thermal conductivity of gas mixtures, because one of future applications of the model is the study of long-term evolution of foam insulation properties. In literature, the thermal conductivity of gas mixtures is often estimated from the conductivities of individual gases using various mixing rules. Although this approach was extensively tested for monoatomic gases and small polyatomic molecules, its precision often suffers for the prediction of conductivity of gas mixtures consisting of larger gas molecules, which are often employed as blowing agents (Dohrn et al., 2007). Accordingly, we compared the predictions of the several frequently used mixing rules and direct molecular dynamics simulations. The conductive–radiative heat transfer in foams is modelled using homogeneous phase approach (Coquard et al., 2011). Polystyrene foams were studied in the literature much more extensively than PU foams. Thus, we mainly focus on typical morphological aspects of PU foams like the strut content.

Under this perspective, the goal of this paper is to develop a multi-scale model capable of predicting the insulation properties of complex materials like PU foams based on first principles with the morphology of the material and the chemical composition of gas and solid phases being the only inputs. Papers usually describe only some aspects of the multi-scale modelling; here, we design and report a multidisciplinary strategy, in which several advanced modelling techniques are combined, yielding a multifaceted, multi-scale description of the phenomena under investigation. The models are coupled together using the MoDeNa platform (MoDeNa-EUProject, 2015). This framework utilizes concept of surrogate models for microscopic codes to enable efficient transfer of information across scales. We compare calculated results with experimental measurements and demonstrate that it is possible to create accurate and efficient predictive tool by linking models from quantum through atomistic to continuum scale.

2. Experimental

2.1. Foam preparation

The chemical components used in PU foam preparation and characterization are reported in Table 1.

The polyurethane foams characterized in this paper were prepared according to the following procedure:

Component A of the reactive foam mixture was obtained by blending polyols and additives such as foam stabilizers (surfactant), catalyst and chemical (water) and physical (cyclopentane) blowing agents in the desired ratio (see Table 2). Component B of the reactive foam mixture was an aromatic isocyanate in all cases.

For the foam preparation component A and B were mixed in a beaker in the specific ratio given in Table 2 using a Vollrath laboratory mixer with a Lenart-disc of diameter 6.5 cm at 1500 rpm for 6 s. The reaction mixture was then poured into a suitable container and left to expand and cure.

2.2. Measurement of equivalent heat conductivity

The equivalent heat conductivity of the foams was measured with a TCA 300 DTX device of the company TAURUS instruments GmbH.

The measurement is based on the principle of heat flow measurement according to ISO 8301.

2.3. Morphological analysis of foams

First, we should emphasize that this work focuses on closed-cell PU foams. Density of the foams ρ_f was determined according to

Table 1
Materials used to prepare the foam samples.

Chemical	Description/Properties	Supplier
Polyol 1	Sucrose based polyether polyol, OH value 400 mg KOH/g	BASF SE
Polyol 2	Glycerol based polyether polyol, OH value 400 mg KOH/g	BASF SE
Polyol 3	Glycerol based polyether polyol, OH value 805 mg KOH/g	BASF SE
Isocyanate	Polymeric MDI, NCO content 31.5%	BASF SE
Surfactant 1	Tegostab B 8467, silicone surfactant	Evonik Goldschmidt
Surfactant 2	Dabco DC 193, silicone surfactant	Air Products
Blowing agent	Cyclo pentane	
Catalyst	N,N-Dimethylcyclohexylamine	

Table 2
Foam formulations. Amounts are given as parts by weight so that the total amount of component A (everything except isocyanate) is equal to 100 parts.

	1-1	1-3	1-5	6-6	6-7	7-2	9-6	10-3	10-6
Polyol 1	80.8	85.3	89.9						
Polyol 2				58.5	59.3	50.2	54.4	57.8	55.4
Polyol 3				34.4	34.8	29.5	32.0	33.9	32.6
Surfactant 1	1.9	2.1	2.2						
Surfactant 2				1.9	1.9	1.6	1.7	1.8	1.8
Catalyst	4.4	4.3	3.6	1.9	1.9	4.0	3.3	2.0	2.3
Water	0.7	0.7	0.8	3.4	2.2			0.9	1.6
Blowing agent	12.1	7.7	3.6			14.7	8.6	3.6	6.3
Isocyanate	89.5	94.5	99.6	182.8	164.7	111.1	120.3	142.0	147.9
Isocyanate index	100	100	100	105	105	105	105	105	105

DIN EN ISO 845. In this paper, we also use foam porosity ε, which is calculated from foam density using

$$\varepsilon = 1 - \frac{\rho_f}{\rho_p}. \tag{1}$$

Here, ρ_p is the polymer density, which has a value of 1100 kg m^{-3} for PU.

X-ray micro-CT scanning was used to create virtual cross-sectional cuts and three-dimensional foam morphologies (see Fig. 1). Although the used apparatus enabled scanning with voxel resolution up to 500 nm, voxel sizes around 2 μm were used in order to maximize the field of view and therefore scan a large number of cells. We cut smaller foam samples (cylinders with 1 cm height and 0.5 cm diameter) in order to speed up the tomography measurements. In this sample, we focused on cylindrical volume with 2 mm height and 2 mm diameter. Analysed samples had 75 complete cells on average. The drawback of this approach is that some parts of the foam walls were thinner than the voxel size, resulting in problems with binarization of the structure as a whole. We found that porosity determined from tomography is usually undervalued by about 1% for PU foams due to limited resolution. Therefore we decided to use porosity calculated from foam density, see Eq. (1). Some of the foam cells then appeared as partially open and the structure had to be re-reconstructed by a post-processing algorithm described by Nistor et al. (2016).

Reconstruction algorithm can be summarized into following steps. First, images are segmented to gas and polymer voxels. Second, images are cleared to remove small artefacts created in segmentation. Third, three-dimensional distance transform is used to identify all cells. Four, watershed algorithm is used to fill the holes in walls. After these steps we have an image of closed-cell foam.

Step-by-step procedure of three-dimensional binary operations was used to delete the cell walls from the binary image, which was implemented in Fiji software (Schindelin et al., 2012). The strut content f_s was then calculated as the ratio between the remaining voxels assigned to struts and the total number of voxels of the foam structure. Thanks to the perfect distinction between cells, the size of each cell could be easily determined. We used the so-called equivalent diameter δ_c, which is defined as the diameter of a sphere with the volume equal to the volume of the respective cell. It should be noted that average cell size determined from CT images is always larger than average cell size determined from SEM images (Nistor et al., 2016).

The wall thickness δ_w and the strut size δ_s needed for the calculation of effective radiative properties in Section 3.4.1 were then calculated from the following system of equations (Placido et al., 2005)

$$V_c = 0.348\delta_s^3, \tag{2a}$$

$$V_s = 2.8\delta_s^2\delta_c - 3.93\delta_s^3, \tag{2b}$$

$$V_w = (1.3143\delta_c^2 - 7.367\delta_s\delta_c + 10.323\delta_s)\delta_w, \tag{2c}$$

$$f_s = \frac{V_s}{V_s + V_w}, \tag{2d}$$

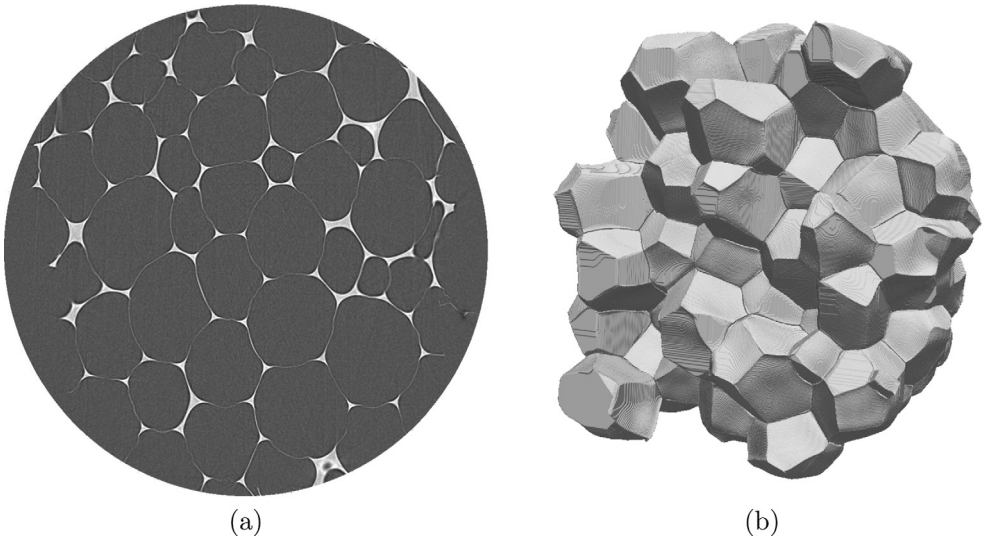

Fig. 1. The picture of (a) cross-sectional cuts and (b) three-dimensional foam morphology of sample 1–3.

$$\frac{\rho_f}{\rho_p} = \frac{V_s + V_w}{V_c}, \tag{2e}$$

This procedure is based on the fact that once the foam density ρ_f, strut content f_s and cell size δ_c are known, wall thickness and strut size can be calculated if we make an assumption on cell shape. Eq. (2) was derived for dodecahedral cells, since it proved to be a reasonable assumption for estimation of heat insulation properties (Coquard and Baillis, 2006). Here, V_c, V_w, V_s are the volumes occupied by gas, walls and struts in a cell, respectively.

3. Theory and mathematical models

3.1. Polymer and gas thermal conductivity by reverse non-equilibrium molecular dynamics (RNEMD)

The thermal conductivity of a rigid polyurethane (PU) polymer k_p and of gaseous mixtures k_g of carbon dioxide (CO_2)/cyclopentane (CyP), CO_2/air (modelled as a mixture of 22% w/w O_2 and 78% w/w N_2), and air/CyP were determined by reverse non-equilibrium molecular dynamics (RNEMD) simulations (Miiller-Plathe, 1997; Zhang et al., 2005).

Generally speaking, NEMD-based procedures involve an artificially imposed external field that drives the system out of equilibrium. In analogy with real experiments, the long-time response to this imposed perturbation is measured to determine the transport property of interest. For instance, in case of thermal conductivity measurements or estimation by NEMD simulations, a temperature gradient is applied to the system and, once the steady state is reached, the corresponding heat flux is measured. In RNEMD, cause and effect are reversed with respect to experiment and conventional NEMD. Thus, in the case of thermal conductivity determination via RNEMD, an exactly known heat flux is imposed on the molecular system under investigation in a given (e.g., z-) direction and the resulting steady-state temperature gradient in the direction parallel to the heat flux is measured.

To perform RENMD-based thermal conductivity estimation, each three-dimensional (3D) periodic simulation box is divided – perpendicularly to the z-direction – into N slabs (where N is an even number) of identical thickness $h = L_z/N$, where L_z is the length of the simulation box in the z-direction. Note that the h must be large enough to contain many particles on average but, at the same time, the condition $h \ll L_z$ must hold. The slab at $z = 0$ acts as heat sink (*the cold zone*) while the one at $z = L_z/2$ acts as heat source (*the hot zone*), respectively. In order to create a heat flux, the non-equilibrium algorithm exchanges the velocity of the fastest particle in the cold slab with the slowest particle in the hot slab with a certain frequency v. Since the energy is conserved, this enforces energy back flow from the hot to the cold slab, which maintains a given temperature gradient related to v. For molecular systems, the exchanged velocities are those of the respective centers-of-mass of the molecules involved in the exchange. Accordingly, old and new velocities before and after any exchange are simply related by: $\mathbf{v}_C^{new} = \mathbf{v}_H^{old}$ and $\mathbf{v}_H^{new} = \mathbf{v}_C^{old}$, where the subscripts C and H denote a molecule in the cold and hot slab, respectively. To enforce invariance of total momentum and total energy of the system under this process, the algorithm must restrict exchange only to particles of the same mass. In order to generalize the application of RNEMD to multicomponent systems independently of the composition, in this work the extension of this original scheme was adopted, as proposed by Nieto-Draghi and Avalos (2003). According to this RNMED generalization scheme, the molecule endowed with the largest kinetic energy (instead of the fastest molecule) in the cold region and the one with the lowest kinetic energy (instead of the slowest molecule) in the hot region are selected, independently of the molecular species present in each slab. By considering momentum and energy exchange between the two selected cold and hot slab particles as if a hypothetical elastic collision between these two molecules would take place, conservation of total momentum and total energy of the systems is preserved. According to this new scheme, after the virtual molecular collision the new velocities of the two molecules in the cold (C) and hot (H) region can be expressed as:

$$\mathbf{v}_C^{new} = -\mathbf{v}_C^{old} + 2\frac{m_C\mathbf{v}_C^{old} + m_H\mathbf{v}_H^{old}}{m_C + m_H} \tag{3}$$

and

$$\mathbf{v}_H^{new} = -\mathbf{v}_H^{old} + 2\frac{m_C\mathbf{v}_C^{old} + m_H\mathbf{v}_H^{old}}{m_C + m_H}, \tag{4}$$

in which m_C and m_H are the masses of the selected particles in the cold (C) and hot (H) slabs, respectively. Of note, the velocities considered in this scheme are the center-of-mass velocities of both species, exchanging their momentum and energy. The energy exchange induced by the virtual collision is summed to the value of the accumulated energy exchanged by the two slabs; from this, it follows that, under steady state, the heat flow induced by this method of exchange can be obtained without distinction from the variation in energy in either of the two slabs, as the sum of all energy transfers per time per area:

$$\langle J_z\rangle(t) = \frac{1}{2At}\sum_{\text{transfers}(t)}\frac{m_H}{2}\left((\mathbf{v}_H^{new})^2 - (\mathbf{v}_H^{old})^2\right), \tag{5}$$

where t is the length of the simulation, A is the cross-sectional area of the simulation box perpendicular to the z-axis (i.e., in the x- and y-directions), and the factor 2 is due to the adopted periodic boundary conditions. Eq. (5) results from the steady state energy balance after the system has been driven out of equilibrium. As such, $\langle J_z\rangle(t)$ corresponds to the macroscopic heat flow measured in real experiments (De Groot and Mazur, 1984; MacGowan and Evans, 1986; Evans and MacGowan, 1987).

Finally, once the thermal gradient is stabilized and the process is stationary, the thermal conductivity can be obtained as:

$$k = \lim_{dT/dz\to 0}\lim_{t\to\infty}\frac{\langle J_z(t)\rangle}{\langle dT/dz\rangle}, \tag{6}$$

where $\langle dT/dz\rangle$ is the resulting temperature gradient in the z-direction. The condition $dT/dz \to 0$ is formally required to ensure that the linear regime is achieved and the classical linear non-equilibrium thermodynamics apply.

In this work, the thermal conductivity k of an optimized rigid PU chain system and of the different gas mixtures was calculated by the RNEMD procedure described above. All simulations were carried out at $T = 283$ K and atmospheric pressure using the COMPASS force field (Sun, 1998), which proved to be extremely accurate in the prediction of thermophysical properties of both condensed and gas phase systems (Cosoli et al., 2007, 2008; Mensitieri et al., 2008; Pricl and Fermeglia, 2003; Milocco et al., 2002; Fermeglia and Pricl, 1999a,b,c).

For the generation of the (PU) polymer, the following general scheme was adopted. Briefly, the molecular model of a PU chain consisting of 4,4′-methylendiisocyanate (MDI) as the hard phase and dipropylene glycol (DPG) as the soft phase was built. Specifically, each polymer had the following structure: DPG–(MDI–DPG)$_n$–H, with $n = 10$ (see Fig. 2a).

The geometry of each polymer chain was optimized (step 1). Next, 10 PU polymer chains were then packed into a simulation box under periodic boundary conditions (see Fig. 2b). 100 different simulation boxes were independently created and, after geometry relaxation of each 3D box, the one with the lowest energy value

was selected (step 2). The selected 3D box containing the polymer chains was subjected to further geometry optimization followed by simulated annealing molecular dynamics (SMD) (8 cycles of 1000 MD steps, temperature range 283–483 K). 5000 steps of classical MD simulations at room temperature 293 K were then carried out to equilibrate the system. All simulations were conducted in the canonical (NVT) ensemble, using an integration time step of 0.2 fs, giving a total annealing time of 1.6 ps, and an overall MD time of 1 ps (step 3). The minimum energy structure was selected for RNEMD simulations (see below).

For the CO_2/air mixture, the entire range of composition (in term of CO_2 mole fraction y_{CO_2}) was simulated in discrete intervals of 0.2 (i.e., y_{CO_2} = 0.00, 0.20, 0.40, 0.60, 0.80, and 1.00). For the two systems involving CyP (i.e., CO_2/CyP and air/CyP), only those systems characterized by a molar fraction of cyclopentane y_{CyP} = 0.00, 0.04, 0.08, 0.16 and 0.20 were simulated, since, according to the corresponding phase diagram, cyclopentane is liquid for $y_{CyP} > 0.25$ at 283 K.

Each RNEMD simulation box consisted in a parallelepiped box with dimensions $L_z = 2L_x = 2L_y$. In the case of gas mixtures, cells were filled with an overall approximately constant number of 1250 molecules, according to each specific mixture compositions described above. Each resulting system was initially subjected to standard equilibrium isothermal isobaric (NPT) MD simulations for 4 ns in order to establish equilibrium densities at 283 K and 1 atm. Subsequently, 1 ns isothermal isochoric (NVT) equilibration runs were conducted using RNEMD, followed by 20 ns production runs, required to achieve a steady linear concentration profile. System temperature was maintained by use of the Berendsen weak-coupling thermostat (Berendsen et al., 1984) (coupling constants $\tau_T = 0.2$ ps). This thermostat was selected since it has been shown previously that this weak thermostat coupling does not significantly affect the calculated thermal conductivity, as the uniform velocity scaling method employed by this thermostat mainly shifts the whole temperature during the simulation profile without inducing other notable alterations (Zhang et al., 2005). The equations of motion were integrated via the leapfrog algorithm with a time step of 2 fs and the application of the SHAKE method (Ryckaert et al., 1977) to constrain bonds to equilibrium value (relative tolerance of 1×10^{-6}). Intermolecular van der Waals interactions were cut off at a distance of 10.0 Å, while long-range electrostatics was treated by Ewald summation (Wells and Chaffee, 2015). To generate the heat flux during the non-equilibrium molecular dynamics simulations, an exchange particle momentum frequency equal to 0.0020 fs^{-1} was selected, since such a value has been shown to allow reaching a reasonable (i.e., not exceedingly large) magnitude of the temperature gradient (Nieto-Draghi and Avalos, 2003).

3.2. Gas mixture conductivity based on mixing rules

One of the goals of the present study is to develop a model, which is able to predict long term evolution of insulation properties of PU foams. Thus, it is imperative that the model is capable of precise prediction of thermal conductivity of gas mixtures.

It is common praxis to use the so-called mixing rules to calculate the thermal conductivity of the mixture from thermal conductivities of pure gases and gas composition. However, there are many different mixing rules in the literature, which provide different results. Thus, we decided to compare the most common mixing rules with the predictions of molecular dynamics and select the most appropriate mixing rules for the system of CO_2–air–cyclopentane.

With the knowledge of pure component conductivities and composition, the easiest to consider is the simple linear mixing rule

$$k_g = \sum_{i=1}^{n} y_i k_{g,i}, \tag{7}$$

where y_i is the molar fraction of the i-th component and n is the number of components.

The rest of the models use the so-called Wassiljewa mixing rules (Wassiljewa, 1904)

$$k_g = \sum_{i=1}^{n} \frac{y_i k_{g,i}}{\sum_{j=1}^{n} y_j A_{ij}}, \tag{8}$$

where A_{ij} are the Wassiljewa coefficients, which are estimated by different models.

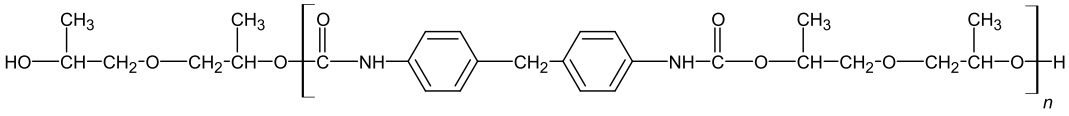

(a)

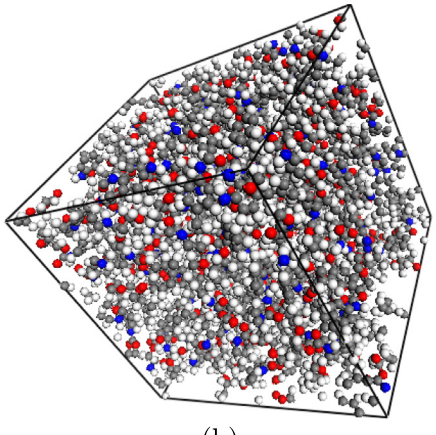

(b)

Fig. 2. (a) Model molecule of PU chain used in RNEMD simulations. (b) 3D atomistic simulation box containing 10 models of PU chains.

Dohrn et al. (2007) defined A_{ij} as

$$A_{ij} = \frac{\left[1 + k_{\mathrm{tr},ij}^{0.5}(M_i/M_j)^{0.25}\right]^2}{\left[8(M_i/M_j)\right]^{0.5}}, \tag{9}$$

where $k_{\mathrm{tr},ij}$ is calculated as

$$k_{\mathrm{tr},ij} = \frac{\Gamma_j\left[\exp(0.0464T_{\mathrm{r},i}) - \exp(-0.2412T_{\mathrm{r},i})\right]}{\Gamma_i\left[\exp(0.0464T_{\mathrm{r},j}) - \exp(-0.2412T_{\mathrm{r},j})\right]}, \tag{10}$$

and where Γ is given by

$$\Gamma = 210\left(\frac{T_c M^3}{p_c^4}\right)^{1/6}. \tag{11}$$

Here, M is the molar mass, T_r is the reduced temperature, T_c is the critical temperature and p_c is the critical pressure.

Lindsay and Bromley (1950) defined A_{ij} as

$$A_{ij} = \frac{1}{4}\left\{1 + \left[\frac{k_{g,i}(c_{p,j} + 1.25R/M_j)}{k_{g,j}(c_{p,i} + 1.25R/M_i)}\left(\frac{M_j}{M_i}\right)^{0.75}\frac{T + S_i}{T + S_j}\right]^{0.5}\right\}^2 \times \frac{T + S_{ij}}{T + S_i}, \tag{12}$$

where R is the gas constant, c_p is the heat capacity, S is the Sutherland constant, which is taken to be

$$S = 1.5T_B, \tag{13}$$

where T_B is the boiling point. Furthermore, S_{ij} is calculated as

$$S_{ij} = \sqrt{S_i S_j}. \tag{14}$$

Mason and Saxena (1958) defined A_{ij} as

$$A_{ij} = \frac{1}{2\sqrt{2}}\left(1 + \frac{M_i}{M_j}\right)^{-0.5}\left[1 + \left(\frac{k_{g,i}E_j}{k_{g,j}E_i}\right)^{0.5}\left(\frac{M_i}{M_j}\right)^{0.25}\right]^2, \tag{15}$$

where E is the Eucken factor, which is given by

$$E = 0.115 + 0.354\frac{c_p}{R}. \tag{16}$$

Finally, Pandey and Prajapati (1979) defined A_{ij} as

$$A_{ij} = \frac{1}{4}\left\{1 + \left[\frac{k_{g,i}}{k_{g,j}}\left(\frac{M_i}{M_j}\right)^{0.25}\frac{T + S_i}{T + S_j}\right]^{0.5}\right\}^2 \frac{T + S_{ij}}{T + S_i}. \tag{17}$$

3.3. Radiative properties of the polymer

Polyurethanes constitute too complex systems to predict their properties with quantum chemical density functional theory (DFT) methods. For this reason, definition of simple, model systems is required. Accordingly, the model molecule used in this work to represent a rigid PU foam is shown in Fig. 3.

It is build up with a central 4,4′-methylene-diphenyl-diisocyanate unit. The isocyanate groups are linked to small poly-propylene-oxide chains, which are cut off after two propylene-oxide monomer units. The rest of the polymer chain is approximated by a methyl group to incorporate the electronic effect of the longer chain into the small model system.

All quantum chemical computations were performed with the TURBOMOLE 6.6 program package (TURBOMOLE, 2007). The geometry of the PU model was optimized at the DFT level of theory (RI-BP86/def-TZVP) (Eichkorn et al., 1995, 1997; Sierka et al., 2003; Treutler and Ahlrichs, 1995; Schafer et al., 1994; Becke, 1988; Perdew, 1986) and the COSMO solvent model ($\epsilon = \infty$) (Klamt and Schuiirmann, 1993). The vibrational normal modes were computed at the same level of theory by using NumForce.

Afterwards the final IR spectrum L was computed by assuming Cauchy-Lorentzian line shapes with a band width s of 5 cm^{-1} (Feller, 1991)

$$L(\omega) = \sum_i \frac{I_i}{\pi}\frac{s}{s^2 + (\omega - \nu_i)^2}. \tag{18}$$

In the formula above, ν_i denotes the wave number of the i-th computed normal mode and I_i its intensity. ω is the frequency of the final IR spectrum L.

The absorption coefficient can be finally calculated as

$$\kappa_p = \frac{L\rho_p}{M_p}, \tag{19}$$

where ρ_p is the density of the polyurethane and $M_p = 544.6$ g mol^{-1} is the molar mass of the model molecule.

3.4. Foam conductivity

The most common method for the prediction of equivalent foam conductivity k_{eq} is the homogeneous phase approach, in which the foam is treated as a homogeneous material with effective conductive and radiative properties. The calculation of effective conductive properties can be based either on simpler analytical methods (Ochsner et al., 2008) or more complex numerical approaches (Coquard and Baillis, 2009; Mendes et al., 2013; Wang and Pan, 2008). In this work, we use analytic model published by Ahern et al. (2005). The methodology for the estimation of effective radiative properties with increasing level of detail was built over the last decade (Placido et al., 2005; Coquard and Baillis, 2006; Coquard et al., 2009, 2013; Kaemmerlen et al., 2010).

Foam conductivity is experimentally determined by the device subjecting the foam sample to a one-dimensional steady-state heat transfer. To determine the equivalent conductivity theoretically, simulation analogous to this experiment is performed. The foam can be treated as a pseudo-homogeneous material with effective conductivity, absorption coefficient and scattering coefficient. In what follows, we will first show, how to determine the effective properties and then how to calculate the equivalent conductivity of the foam.

3.4.1. Effective properties

Effective foam conductivity represents how efficiently foam transfers heat by conduction. It depends on foam morphology

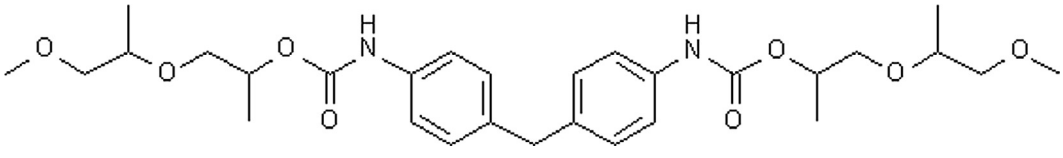

Fig. 3. Model molecule of polyurethane used to predict the absorption coefficient.

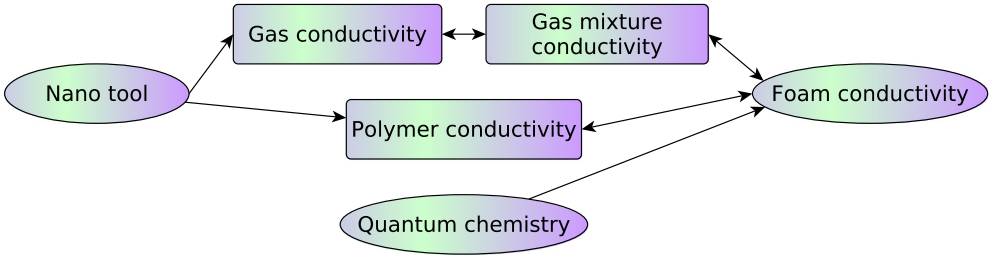

Fig. 4. Schematic diagram of the complete multi-scale simulation. The elliptical shape represents the detailed model, whereas the rectangular shape represents the surrogate model.

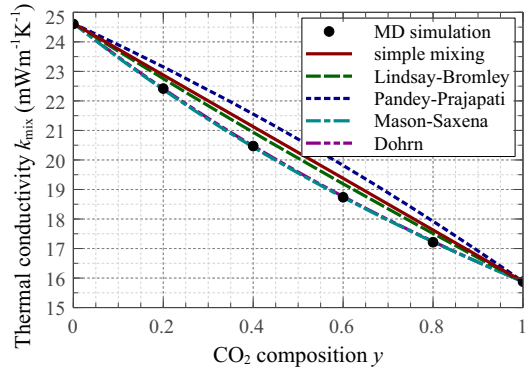

(a)

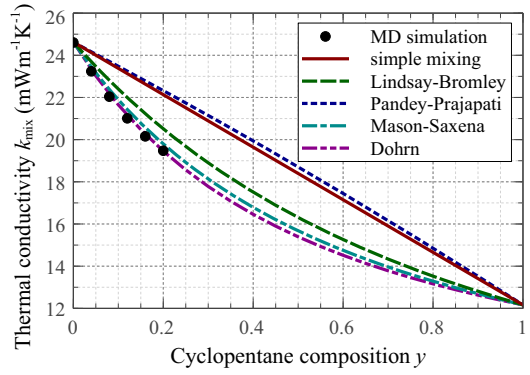

(b)

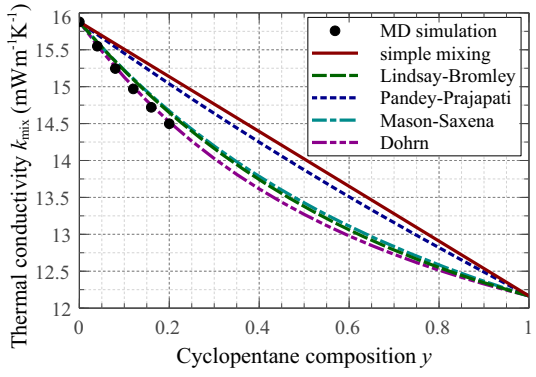

(c)

Fig. 5. Thermal conductivity of binary gas mixtures at 283 K: (a) CO_2–air, (b) cyclopentane–air, (c) cyclopentane–CO_2.

and conductivity of gas and polymer. Ahern et al. (2005) showed that k_f can be calculated as

$$k_f = \frac{k_g\varepsilon + k_p(1-\varepsilon)X}{\varepsilon + (1-\varepsilon)X}, \tag{20}$$

where ε is the foam porosity and X is defined as

$$X = (1-f_s)X_w + f_sX_s, \tag{21}$$

where f_s is the strut content and X_w and X_s are calculated as

$$X_w = \frac{2}{3}\left(1 + \frac{k_g}{2k_p}\right), \tag{22a}$$

$$X_s = \frac{1}{3}\left(1 + \frac{4k_g}{k_g + k_p}\right). \tag{22b}$$

The effective radiative properties can be calculated under the assumption of independent scattering of struts and walls. It is assumed that the foam contains randomly oriented walls, which are modelled as slabs, and randomly oriented struts, which are modelled as long cylinders. The number and cross-sectional area of walls and struts in the unit volume is related to the idealized foam containing dodecahedral cells. The derivation of the equations can be found elsewhere (Dombrovsky and Baillis, 2010). Kaemmerlen et al. (2010) studied the effect of strut shape on radiative properties and provided a correction factor, which can be used to calculate radiative properties of more realistically shaped struts instead of long cylinders. Thus, the transport extinction coefficient can be written as

$$\beta_f^{tr} = (1-f_s)\beta_w^{tr} + f_s\beta_s^{tr}, \tag{23}$$

where β_w^{tr} is calculated as

$$\beta_w^{tr} = \frac{\rho_f}{2\delta_w\rho_p}\int_0^{\frac{\pi}{2}} [R(\alpha,m)\cos(2\alpha) + 1 - T(\alpha,m)]\sin(2\alpha)\,\mathrm{d}\alpha, \tag{24}$$

and β_s^{tr} is calculated as

$$\beta_s^{tr} = \frac{4\rho_f}{\pi\delta_s\rho_p} \times \int_0^{\frac{\pi}{2}} \left[Q_e(\phi,m) - Q_s(\phi,m)\sin^2\phi - g_{cyl}(\phi,m)Q_e(\phi,m)\sin^2\phi\right]\cos\phi\,\mathrm{d}\phi. \tag{25}$$

Here ρ_f is the foam density, ρ_p is the polymer density, δ_w is the wall thickness, α is the angle of incidence to the wall, R is the wall reflectance, T is the wall transmittance, ϕ is the angle of incidence to the strut, g_{cyl} is the anisotropy factor and Q_e and Q_s are the extinction and scattering efficiencies of the strut. Reflectance and transmittance can be calculated using the geometrical optics approximation (Modest, 2003). Anisotropy factor and extinction and scattering coefficients can be calculated using the Mie theory (Dombrovsky and Baillis, 2010).

3.4.2. Equivalent conductivity

The equivalent conductivity represents how efficiently foam transfers heat by both conduction and radiation. The steady-state energy balance in the foam in this case can be written as

$$\nabla\cdot(\mathbf{q}_{tot}) = \nabla\cdot(\mathbf{q}_{con} + \mathbf{q}_{rad}) = 0, \tag{26}$$

where $\mathbf{q}_{tot}, \mathbf{q}_{con}, \mathbf{q}_{rad}$ are the total, conductive and radiative heat flux, respectively.

When the foam is viewed as a pseudo-homogeneous material, the conductive heat flux is expressed as

$$\mathbf{q}_{con} = -k_f \nabla T, \tag{27}$$

where T is the temperature and k_f is the effective conductivity of the foam.

The divergence of the radiative heat flux is written as (Modest, 2003)

$$\nabla \cdot \mathbf{q}_{rad} = \int_0^\infty \kappa_{f\lambda}(4E_{b\lambda} - G_\lambda)\, d\lambda, \tag{28}$$

where $\kappa_{f\lambda}$ is the absorption coefficient of the foam, $E_{b\lambda}$ is the blackbody emissive power, G_λ is the incident radiation and λ is the wavelength.

The evaluation of Eq. (28) requires the prior solution of radiative transfer equation (RTE), which is an integro-differential equation, and thus difficult to solve numerically. In engineering practice, the RTE is usually reduced using the P_1-approximation, discrete ordinate method or the zonal method. The advantages and disadvantages of these methods are well documented elsewhere (Modest, 2003). In this work, we chose to use the P_1-approximation and the stepwise gray box model to deal with the spectral dependence of the emissive power and incidence radiation. Using these methods, Eq. (26) is rewritten as (Mazumder, 2005)

$$k_f \nabla^2 T = \sum_{k=1}^{N} \kappa_{fk}(4E_{bk} - G_k) \tag{29}$$

subjected to boundary conditions

$$T|_{x=0} = T_0, \tag{30a}$$
$$T|_{x=L} = T_L, \tag{30b}$$

where N is the number of spectral boxes and T_0 and T_L are the temperatures of the boundaries.

The incident radiation is calculated from (Mazumder, 2005)

$$\nabla \cdot \left(\frac{1}{\beta_{fk}^{tr}} \nabla G_k \right) = -3\kappa_{fk}(4E_{bk} - G_k) \quad \forall k = 1, 2, \ldots, N, \tag{31}$$

subjected to boundary conditions

$$\left.\frac{dG}{dx}\right|_{x=0} = -\frac{3}{2}\frac{\epsilon_0}{2-\epsilon_0}\kappa_{fk}(4E_{bk}|_{x=0} - G_k|_{x=0}), \tag{32a}$$
$$\left.\frac{dG}{dx}\right|_{x=L} = \frac{3}{2}\frac{\epsilon_L}{2-\epsilon_L}\kappa_{fk}(4E_{bk}|_{x=L} - G_k|_{x=L}), \tag{32b}$$

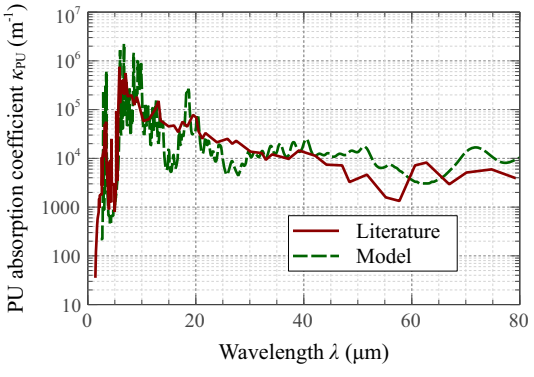

Fig. 6. Comparison of measured and calculated absorption coefficient of polyurethane.

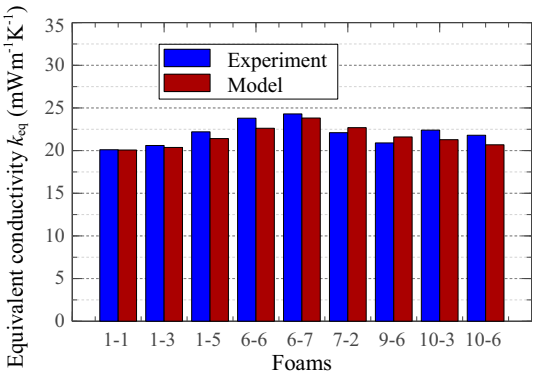

Fig. 7. Comparison of measured and calculated equivalent conductivity of prepared foam samples.

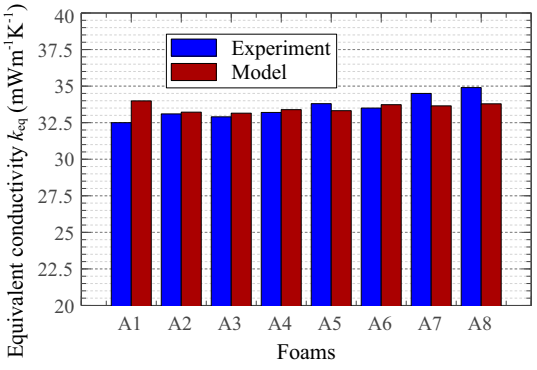

Fig. 8. Comparison of measured and calculated equivalent conductivity of foam samples from Ahern et al. (2005).

where $\sigma_{f\lambda}$ is the scattering coefficient of the foam and ϵ_0 and ϵ_L are the emissivities of the boundaries.

The blackbody emissive power is calculated as (Mazumder, 2005)

$$E_{bk} = [f(\lambda_{k1}, T) - f(\lambda_{k2}, T)]\sigma_B T^4, \tag{33}$$

where σ_B is the Stefan-Boltzmann constant, f is the so-called fraction of blackbody radiation, which can be calculated using a power series (Siegel and Howell, 2002) and λ_{k1} and λ_{k2} are the upper and lower bounds of the k-th box.

Eqs. (29) and (31) represent a system of $N+1$ coupled partial differential equations. Its solution provides the spatial distribution of temperature and incident radiation. Total heat flux can be calculated from (Modest, 2003)

$$q_t = -k_f \frac{dT}{dx} - \sum_{k=1}^{N} \frac{1}{3\beta_{fk}^{tr}} \frac{dG}{dx}. \tag{34}$$

Finally, the equivalent conductivity of the foam is then calculated as

$$k_{eq} = \frac{q_t L}{T_L - T_0}. \tag{35}$$

3.5. Model coupling

The schematic diagram of the entire multi-scale simulation strategy is shown in Fig. 4. The direct coupling between molecular dynamics and model for the prediction of foam conductivity would not be computationally feasible. Thus, we used the MoDeNa software (MoDeNa-EUProject, 2015) to link the individual models.

Table 3
Morphological data of prepared foam samples.

Foam	ρ_f (kg m^{-3})	ε	δ_c (μm)	f_s	y_{CO_2}	y_{CyP}
1-1	35.4	0.968	510	0.63	0.18	0.82
1-3	49.3	0.955	430	0.72	0.27	0.73
1-5	71.4	0.935	340	0.85	0.45	0.55
6-6	37.2	0.966	380	0.62	1.00	0.00
6-7	56.0	0.949	402	0.75	1.00	0.00
7-2	37.9	0.966	899	0.72	0.00	1.00
9-6	55.9	0.949	619	0.80	0.00	1.00
10-3	66.1	0.940	345	0.82	0.50	0.50
10-6	39.8	0.964	460	0.68	0.50	0.50

Table 4
Morphological data of foam samples from Ahern et al. (2005).

Foam	ρ_f (kg m^{-3})	ε	δ_c (μm)	f_s	y_{Air}
A1	38.9	0.965	500	0.954	1.00
A2	47.5	0.957	478	0.922	1.00
A3	58.4	0.947	465	0.914	1.00
A4	64.2	0.942	445	0.923	1.00
A5	66.7	0.939	436	0.909	1.00
A6	69.6	0.937	425	0.949	1.00
A7	77.3	0.930	390	0.935	1.00
A8	85.0	0.923	353	0.942	1.00

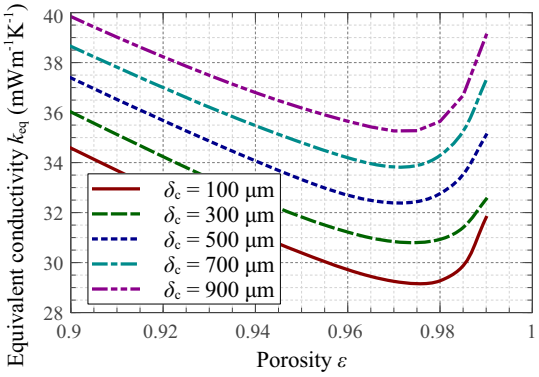

Fig. 9. The dependence of equivalent conductivity k_{eq} on the porosity and cell size. The strut content was $f_s = 0.8$ and the cells were filled with air.

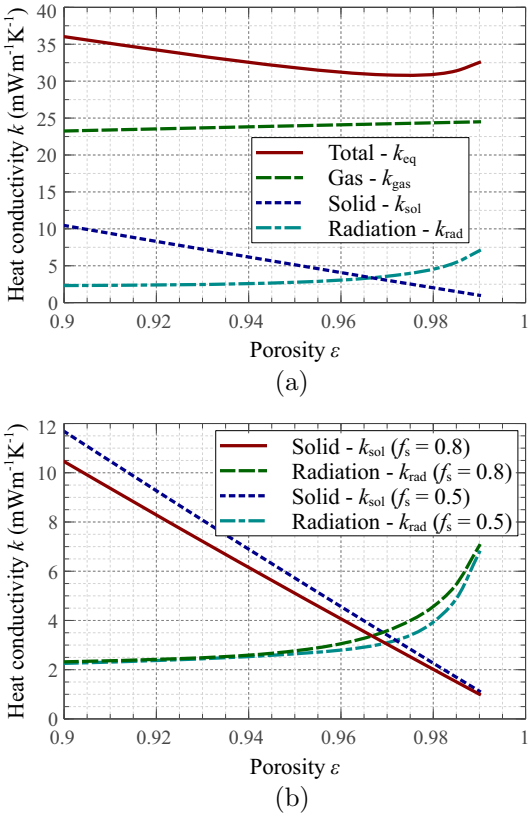

Fig. 10. The dependence of heat conductivity on (a) porosity and (b) porosity and strut content. The strut content was $f_s = 0.8$, the cell size was $\delta_c = 300$ μm and the cells were filled with air.

The framework introduces the concept of the surrogate models. These simplified models must have the form of explicit algebraic equation with free parameters to ensure fast evaluation. The surrogate model and its parameters are stored in a dedicated database and the communication between the models is enabled using simple python adaptors. Thus, when the higher-scale model needs to use property calculated by the lower-scale model, it actually evaluates the surrogate model instead of the complex and time-consuming lower-scale application. The MoDeNa software provides tools for the automatic fitting of the free parameters of the surrogate models to the results of the lower-scale application. Moreover, the framework checks that the surrogate model is not used in the region, which has not been explored by the complex lower-scale application yet.

In this work, the "Nano tool" in Fig. 4 is the MD software described in Section 3.1, which is used to calculate thermal conductivity of phases. A surrogate model is created for each species (denoted as "Gas conductivity" and "Polymer conductivity" in Fig. 4). We used simple linear dependence on temperature for these models

$$k = a + bT, \tag{36}$$

where a and b are the free parameters. To avoid creating an adaptor between each gas conductivity surrogate model and "Foam conductivity" application (described in Section 3.4), we introduced the model (denoted as "Gas mixture conductivity" in Fig. 4), which implements models described in Section 3.2. Thus, we can evaluate thermal conductivity of gas mixture in "Foam conductivity"

application using just the temperature and composition of the gas mixture.

4. Results and discussion

We compared thermal conductivities predicted by several gas mixture models from Section 3.2 for three binary mixtures, which are relevant for PU foams (see Fig. 5). It can be seen that the simple mixing and Pandey-Prajapati models generally predict higher values of thermal conductivity than the rest of the models. The predictions of all models for CO_2–air and cyclopentane–CO_2 mixtures were within 5.4%. The largest difference between model predictions was found for cyclopentane–air mixture, which was as large as 18% This is most likely caused by the large difference in molecular weight between cyclopentane and air molecules.

We also performed RNEMD simulations for the same binary mixtures to decide, which of the investigated gas mixture models provides most accurate results. It can be seen in Fig. 5 that Dohrn model provides the best results for gas mixtures of our interest. Thus, Dohrn model was used as the surrogate model for gas mixtures in this work.

Nielsen et al. (2000) determined that PU polymer has thermal conductivity 0.19–0.21 W m^{-1} K^{-1} depending on formulation. This corresponds well with the value of 0.187 W m^{-1} K^{-1} calculated using RNEMD simulations for 283 K. It should be noted that 10% difference in polymer conductivity has only minor effect on foam conductivity, because the conduction through polymer matrix creates only about 5% of the total heat flux.

The ability of the polyurethane to absorb the thermal radiation can be expressed by the absorption coefficient. We calculated this property using the model described in Section 3.3. The calculated absorption coefficient shown in Fig. 6 is in a good agreement with the experimental value taken from literature (Dombrovsky and Baillis, 2010).

The calculated foam equivalent conductivity was compared with experimental data for foam samples prepared in this study (see Fig. 7) and for experimental data published by Ahern et al. (2005) (see Fig. 8). All information about foam samples is summarized in Tables 3 and 4, respectively. It can be seen that the experimental and predicted data agree very well regardless of foam density or cell size.

Fig. 9 shows the dependence of equivalent conductivity on porosity and cell size. For all cell sizes one can find the optimum porosity, at which the equivalent conductivity is minimal. This is caused by the competition between the conductive and radiative heat transfer. The conductive heat flux decreases with increasing porosity, because the high-conducting polymer is being replaced by low-conducting air. On the other hand, the radiative heat flux increases with increasing porosity, because the lower solid content leads to less absorption of the thermal radiation. The contributions of radiation, and conduction through gas and solid matrix to the overall heat transfer are traditionally expressed by conductivities k_{rad}, k_{gas}, and k_{sol} (see Fig. 10), which are related together by

$$k_{eq} = k_{rad} + k_{sol} + k_{gas}. \tag{37}$$

In Fig. 10, the conductivity through gas phase k_{gas} remains practically constant in the investigated porosity range, because there is only 10% increase in the amount of gas phase in the foam. The conductivity through solid matrix k_{sol} decreases with increasing porosity and increasing strut content. Strut content is the ratio of volume of polymer in struts and total volume of polymer in foam. Foam with low strut content transfers heat more efficiently by conduction, because more of the solid phase is located parallel to the heat flux (Ochsner et al., 2008). And finally, radiative conductivity k_{rad} increases with increasing porosity and strut content in the investigate range (see also Fig. 11).

It is interesting to note that at a f_s value of 0.8 a minimum in equivalent conductivity is obtained at a porosity of 0.975, irrespective of the cell size. The porosity of 0.975 corresponds to a foam density of 27.5 kg m^{-3}.

Reducing the cell size in PU foams leads to lower equivalent conductivity in contrast with polystyrene (EPS) foams, where the opposite trend is observed (Schellenberg and Wallis, 2010; Ferkl et al., 2014). This can be attributed to the much higher absorption coefficient of the polyurethane matrix material.

Polyurethane foams contain a significant part of the solid phase in the struts. A decrease in strut content would improve the mechanical strength of the foams, but its effect on insulation properties of foams is difficult to predict without the mathematical model. Fig. 11 shows the calculated dependence of equivalent conductivity of PU foams as a function of the strut content. An increase in strut content decreases the conductive heat flux. However, increasing the strut content too much leads to very thin walls, which are not very effective at attenuating the radiation. Consequently the radiation heat flux increases again with increasing values of f_s.

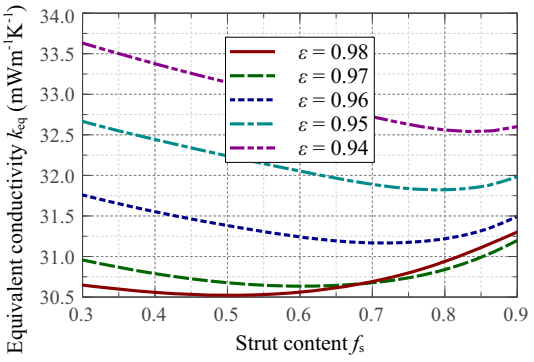

Fig. 11. The dependence of equivalent conductivity k_{eq} on the porosity and strut content. The cell size was $\delta_c = 300$ μm and the cells were filled with air.

5. Conclusions

We presented a multi-scale model for the prediction of heat insulation properties of PU foams. The model is based on first principles and takes only foam morphology and cell gas composition as inputs. The time consuming Quantum chemical and Molecular dynamics computations are efficiently coupled with the simulation of heat transfer in foams using suitable surrogate models within the MoDeNa framework. We compared several mixing rules and showed that Dohrn model is most suitable for the considered blowing agents. Using the developed model we demonstrated the influence of foam morphology and cell gas composition on heat insulation properties of PU foams and we highlighted the differences between PU and EPS foams. We verified the accuracy of the model by successfully validating its predictions against experimental measurements on several in house generated foam samples as well as literature data. Although this paper is focused on PU foams, the methodology is applicable to other types of foams as well. Encouraged by the present results, we are focusing our current efforts on expanding our approach to the simulation of ageing of PU foam heat insulation properties.

Acknowledgments

The research leading to these results has received funding from the European Community's Seventh Framework Programme

(FP7/2007-2013) under grant agreement no [604271]. The financial support from specific university research (MSMT No 20-SVV/2017) is gratefully acknowledged. We also thank our colleagues, Henrik Rusche and Sigve Karolius, who provided supports on the application of MoDeNa framework.

References

Ahern, A., Verbist, G., Weaire, D., Phelan, R., Fleurent, H., 2005. The conductivity of foams: a generalisation of the electrical to the thermal case. Colloids Surf., A 263 (1–3), 275–279. http://dx.doi.org/10.1016/j.colsurf a.2005.01.026. ISSN: 09277757 <http://linkinghub.elsevier.com/retrieve/pii/S0927775705000920>.

Becke, A.D., 1988. Density-functional exchange-energy approximation with correct asymptotic behavior. Phys. Rev. A 38 (6), 3098–3100. http://dx.doi.org/10.1103/PhysRevA.38.3098. ISSN: 0556-2791 <http://link.aps.org/doi/10.1103/PhysRevA.38.3098>.

Berendsen, H.J.C., Postma, J.P.M., van Gunsteren, W.F., DiNola, A., Haak, J.R., 1984. Molecular dynamics with coupling to an external bath. J. Chem. Phys. 81 (8), 3684. http://dx.doi.org/10.1063/1.448118. ISSN: 00219606 <http://scitation.aip.org/content/aip/journal/jcp/81/8/10.1063/1.448118>.

Coquard, R., Baillis, D., 2006. Modeling of heat transfer in low-density EPS foams. J. Heat Transfer 128 (6), 538–549. http://dx.doi.org/10.1115/1.2188464. ISSN: 00221481 <http://heattransfer.asmedigitalcollection.asme.org/article.aspx?articleid=1448362>.

Coquard, R., Baillis, D., 2009. Numerical investigation of conductive heat transfer in high-porosity foams. Ada Mater. 57 (18), 5466–5479. http://dx.doi.org/10.1016/j.actamat.2009.07.044. ISSN: 13596454 <http://linkinghub.elsevier.com/retrieve/pii/S1359645409004789>.

Coquard, R., Baillis, D., Randrianalisoa, J., 2011. Homogeneous phase and multi-phase approaches for modeling radiative transfer in foams. Int. J. Therm. Sci. 50 (9), 1648–1663. http://dx.doi.org/10.1016/j.ijthermalsci.2011.04.012. ISSN: 12900729 <http://linkinghub.elsevier.com/retrieve/pii/S129007291100130X>.

Coquard, Remi, Baillis, Dominique, Quenard, Daniel, 2009. Radiative properties of expanded polystyrene foams. J. Heat Transfer 131 (1), 012702. http://dx.doi.org/10.1115/1.2994764. ISSN: 00221481 <http://heattransfer.asmedigitalcollection.asme.org/article.aspx?articleid=1449450>.

Coquard, Remi, Randrianalisoa, Jaona, Baillis, Dominique Doermann, 2013. Computational prediction of radiative properties of polymer closed-cell foams with random structure. J. Porous Media 16 (2), 137–154. http://dx.doi.org/10.1615/JPorMedia.vl6.i2.50. ISSN: 1091-028X <http://www.dl.begellhouse.com/journals/49dcde6d4c0809db,65dlf2aO716e7f48,3618b54d4687e2b0.html>.

Cosoli, P., Ferrone, M., Pricl, S., Fermeglia, M., 2008. Hydrogen sulfide removal from biogas by zeolite adsorption. Part II. MD simulations. Chem. Eng. J. 145 (1), 93–99. http://dx.doi.org/10.1016/j.cej.2008.08.013. ISSN: 13858947 <http://linkinghub.elsevier.com/retrieve/pii/S1385894708005160>.

Cosoli, Paolo, Ferrone, Marco, Pricl, Sabrina, Fermeglia, Maurizio, 2007. Grand Canonical Monte-Carlo simulations for VOCs adsorption in non-polar zeolites. Int. J. Environ. Technol. Manage. 7 (1/2), 228. http://dx.doi.org/10.1504/IJETM.2007.013247. ISSN: 1466-2132 <http://www.inderscience.com/link.php?id=13247>.

De Groot, S.R., Mazur, P., 1984. Non-equilibrium Thermodynamics. Dover Press, New York.

Dohrn, Ralf, Fonseca, Jose M., Albers, Reinhard, Kusan-Bindels, Jacqueline, Marrucho, Isabel M., 2007. Thermal conductivity of polyurethane foam cell gases: improved transient hot wire cell – data of isopentane + n-pentane mixtures – extended Wassiljewa-model. Fluid Phase Equilib. 261 (1–2), 41–49. http://dx.doi.org/10.1016/j.fluid.2007.07.059. ISSN: 03783812 <http://linkinghub.elsevier.com/retrieve/pii/S0378381207003743>.

Dombrovsky, Leonid A., Baillis, Dominique, 2010. Thermal Radiation in Disperse Systems: An Engineering Approach. Begell House, p. 689. ISBN: 978-567000-268-3.

Eichkorn, K., Treutler, O., Ohm, H., Haser, M., Ahlrichs, R., 1995. Auxiliary basis sets to approximate Coulomb potentials (Chem. Phys. Lett. 240 (1995) 283–290). Chem. Phys. Lett. 242 (6), 652–660. http://dx.doi.org/10.1016/0009-2614(95)00838-U. ISSN: 00092614 <http://linkinghub.elsevier.com/retrieve/pii/000926149500838U>.

Eichkorn, Karin, Weigend, Florian, Treutler, Oliver, Ahlrichs, Reinhart, 1997. Auxiliary basis sets for main row atoms and transition metals and their use to approximate Coulomb potentials. Theor. Chem. Acc.: Theory, Comput., Model. (Theor. Chim. Ada) 97 (1–4), 119–124. http://dx.doi.org/10.1007/S002140050244. ISSN: 1432-881X <http://link.springer.com/10.1007/s002140050244>.

Evans, Denis J., MacGowan, David, 1987. Addendum to heat and matter transport in binary liquid mixtures. Phys. Rev. A 36 (2), 948–950. http://dx.doi.org/10.1103/PhysRevA.36.948. ISSN: 0556-2791 <http://link.aps.org/doi/10.1103/PhysRevA.36.948>.

Feller, William, 1991. An Introduction to Probability Theory and Its Applications: 2. John Wiley & Sons. ISBN: 0-471-25709-5.

Ferkl, Pavel, Pokorny, Richard, Kosek, Juraj, 2014. Multiphase approach to coupled conduction-radiation heat transfer in reconstructed polymeric foams. Int. J. Therm. Sci. 83, 68–79. http://dx.doi.org/10.1016/j.ijthermalsci.2014.04.013. ISSN: 12900729 <http://linkinghub.elsevier.com/retrieve/pii/S1290072914001008>.

Fermeglia, Maurizio, Pricl, Sabrina, 1999a. A novel approach to thermophysical properties prediction for chloro-fluoro-hydrocarbons. Fluid Phase Equilib. 166 (1), 21–37. http://dx.doi.org/10.1016/S0378-3812(99)00295-2. ISSN: 03783812 <http://linkinghub.elsevier.com/retrieve/pii/S0378381299002952>.

Fermeglia, Maurizio, Pricl, Sabrina, 1999b. Molecular dynamics simulations of real systems: application to chloro-fluoro-hydrocarbons and polymers. Fluid Phase Equilib. 158–160, 49–58. http://dx.doi.org/10.1016/S0378-3812(99)00093-X. ISSN: 03783812 <http://linkinghub.elsevier.com/retrieve/pii/S037838129900093X>.

Fermeglia, Maurizio, Pricl, Sabrina, 1999c. Equation-of-state parameters for pure polymers by molecular dynamics simulations. AIChE J. 45 (12), 2619–2627. http://dx.doi.org/10.1002/aic.690451218. ISSN: 00011541 <http://doi.wiley.com/10.1002/aic.690451218>.

Kaemmerlen, A., Vo, C., Asllanaj, F., Jeandel, G., Baillis, D., 2010. Radiative properties of extruded polystyrene foams: predictive model and experimental results. J. Quant. Spectrosc. Radiat. Transfer 111 (6), 865–877. http://dx.doi.org/10.1016/j.jqsrt.2009.11.018. ISSN: 00224073 <http://linkinghub.elsevier.com/retrieve/pii/S0022407309003616>.

Klamt, A., Schuiirmann, G., 1993. COSMO: a new approach to dielectric screening in solvents with explicit expressions for the screening energy and its gradient. J. Chem. Soc., Perkin Trans. 2 5, 799–805. http://dx.doi.org/10.1039/P29930000799. ISSN: 0300-9580 <http://xlink.rsc.org/?DOI=P29930000799>.

Klempner, Daniel, Sendijarevic, Vahid, Mikhailovna Aseeva, Roza, 2004. Handbook of Polymeric Foams and Foam Technology. Hanser Gardener Publications, p. 584. ISBN: 1569903360.

Lindsay, Alexander L., Bromley, LeRoy A., 1950. Thermal conductivity of gas mixtures. Ind. Eng. Chem. 42 (8), 1508–1511. http://dx.doi.org/10.1021/ie50488a017. ISSN: 0019-7866 <http://pubs.acs.org/doi/abs/10.1021/ie50488a017>.

MacGowan, David, Evans, Denis J., 1986. Heat and matter transport in binary liquid mixtures. Phys. Rev. A 34 (3), 2133–2142. http://dx.doi.org/10.1103/PhysRevA.34.2133. ISSN: 0556-2791 <http://link.aps.org/doi/10.1103/PhysRevA.34.2133>.

Mason, E.A., Saxena, S.C., 1958. Approximate formula for the thermal conductivity of gas mixtures. Phys. Fluids 1 (5), 361. http://dx.doi.org/10.1063/1.1724352. ISSN: 00319171 <http://scitation.aip.org/content/aip/journal/pof1/1/5/10.1063/1.1724352>.

Mazumder, Sandip, 2005. A new numerical procedure for coupling radiation in participating media with other modes of heat transfer. J. Heat Transfer 127 (9), 1037. http://dx.doi.org/10.1115/1.1929780. ISSN: 00221481 <http://link.aip.org/link/JHTRAO/vl27/i9/pl037/sl%7B%5C&%7DAgg=doi>.

Mendes, Miguel A.A., Ray, Subhashis, Trimis, Dimosthenis, 2013. A simple and efficient method for the evaluation of effective thermal conductivity of open-cell foam-like structures. Int. J. Heat Mass Transfer 66, 412–422. http://dx.doi.org/10.1016/j.ijheatmasstransfer.2013.07.032. ISSN: 00179310 <http://linkinghub.elsevier.com/retrieve/pii/S0017931013005863>.

Mensitieri, Giuseppe, Larobina, Domenico, Guerra, Gaetano, Venditto, Vincenzo, Fermeglia, Maurizio, Pricl, Sabrina, 2008. Chloroform sorption in nanoporous crystalline and amorphous phases of syndiotactic polystyrene. J. Polym. Sci., Part B: Polym. Phys. 46 (1), 8–15. http://dx.doi.org/10.1002/polb.21303. ISSN: 08876266 <http://doi.wiley.com/10.1002/polb.21303>.

Mills, Nigel J., 2007. Polymer Foams Handbook: Engineering and Biomechanics Applications and Design Guide. Butterworth-Heinemann, p. 531. ISBN: 0750680695.

Milocco, Oliver, Fermeglia, Maurizio, Pricl, Sabrina, 2002. Prediction of thermophysical properties of alternative refrigerants by computational chemistry. Fluid Phase Equilib. 199 (1–2), 15–21. http://dx.doi.org/10.1016/S0378-3812(01)00811-1. ISSN: 03783812 <http://linkinghub.elsevier.com/retrieve/pii/S0378381201008111>.

MoDeNa-EUProject, 2015. Modelling of Morphology DEvelopment of Micro-and NAnostructures. <https://github.com/MoDeNa-EUProject/MoDeNa>.

Modest, M.F., 2003. Radiative Heat Transfer. Academic Press, p. 845. ISBN: 0125031637.

Miiller-Plathe, Florian, 1997. A simple nonequilibrium molecular dynamics method for calculating the thermal conductivity. J. Chem. Phys. 106 (14), 6082. http://dx.doi.org/10.1063/1.473271. ISSN: 00219606 <http://scitation.aip.org/content/aip/journal/jcp/106/14/10.1063/1.473271>.

Nielsen, Lars, Ebert, Hans-Peter, Hemberger, Frank, Fricke, Jochen, Biedermann, Anja, Reichelt, Michael, Rotermund, Udo, 2000. Thermal conductivity of nonporous polyurethane. High Temp.-High Press. 32 (6), 701–707. http://dx.doi.org/10.1068/htwu69. ISSN: 0018-1544 <http://www.hthpweb.com/abstract.cgi?id=htwu69>.

Nieto-Draghi, Carlos, Avalos, Josep Bonet, 2003. Non-equilibrium momentum exchange algorithm for molecular dynamics simulation of heat flow in multicomponent systems. Mol. Phys. 101 (14), 2303–2307. http://dx.doi.org/10.1080/0026897031000154338. ISSN: 0026-8976 <http://www.tandfonline.com/doi/abs/10.1080/00268970310001543338>.

Nistor, Andra, Toulec, Milos, Zubov, Alexandr, Kosek, Juraj, 2016. Tomographic reconstruction and morphological analysis of rigid polyurethane foams.

Macromol. Symp. 360 (1), 87–95. http://dx.doi.org/10.1002/masy.201500113. ISSN: 10221360 <http://doi.wiley.com/10.1002/masy.201500113>.
Ochsner, Andreas, Murch, Graeme A., de Lemos, Marcelo J.S., 2008. Cellular and Porous Materials. Wiley, p. 439. ISBN: 978-3-527-31938-1 <http://eu.wiley.com/WileyCDA/WileyTitle/productCd-3527319387,subjectCd-PH80.html>.
Pandey, J.D., Prajapati, S.R., 1979. A new method for the calculation of thermal conductivity of binary gas mixtures. Proc. Indian Natl. Sci. Acad. 45 (5), 372–382.
Perdew, John P., 1986. Density-functional approximation for the correlation energy of the inhomogeneous electron gas. Phys. Rev. B 33 (12), 8822–8824. http://dx.doi.org/10.1103/PhysRevB.33.8822. ISSN: 0163-1829 <http://link.aps.org/doi/10.1103/PhysRevB.33.8822>.
Placido, E., Arduini-Schuster, M.C., Kuhn, J., 2005. Thermal properties predictive model for insulating foams. Infrared Phys. Technol. 46 (3), 219–231. http://dx.doi.org/10.1016/j.infrared.2004.04.001. ISSN: 13504495 <http://linkinghub.elsevier.com/retrieve/pii/S1350449504000702>.
Pricl, Sabrina, Fermeglia, Maurizio, 2003. Atomistic molecular dynamics simulations of gas diffusion and solubility in rubbery amorphous hydrocarbon polymers. Chem. Eng. Commun. 190 (10), 1267–1292. http://dx.doi.org/10.1080/00986440302153. ISSN: 0098-6445 <http://www.tandfonline.com/doi/abs/10.1080/00986440302153>.
Ryckaert, Jean-Paul, Ciccotti, Giovanni, Berendsen, Herman J.C., 1977. Numerical integration of the cartesian equations of motion of a system with constraints: molecular dynamics of *n*-alkanes. J. Comput. Phys. 23 (3), 327–341. http://dx.doi.org/10.1016/0021-9991(77)90098-5. ISSN: 00219991 <http://linkinghub.elsevier.com/retrieve/pii/0021999177900985>.
Schafer, Ansgar, Huber, Christian, Ahlrichs, Reinhart, 1994. Fully optimized contracted Gaussian basis sets of triple zeta valence quality for atoms Li to Kr. J. Chem. Phys. 100 (8), 5829. http://dx.doi.org/10.1063/1.467146. ISSN: 00219606 <http://scitation.aip.org/content/aip/journal/jcp/100/8/10.1063/1.467146>.
Schellenberg, J., Wallis, M., 2010. Dependence of thermal properties of expandable polystyrene particle foam on cell size and density. J. Cell. Plast. 46 (3), 209–222. http://dx.doi.org/10.1177/0021955X09350803. ISSN: 0021-955X <http://cel.sagepub.com/cgi/doi/10.1177/0021955X09350803>.
Schindelin, Johannes et al., 2012. Fiji: an open-source platform for biological-image analysis. Nat. Methods 9 (7), 676–682. http://dx.doi.org/10.1038/nmeth.2019. ISSN: 1548-7091 <http://www.nature.com/doifinder/10.1038/nmeth.2019>.
Siegel, R., Howell, J.R., 2002. Thermal Radiation Heat Transfer, vol. 111. Taylor & Francis. xxvi, 868 p. ISBN: 1560328398.
Sierka, Marek, Hogekamp, Annika, Ahlrichs, Reinhart, 2003. Fast evaluation of the Coulomb potential for electron densities using multipole accelerated resolution of identity approximation. J. Chem. Phys. 118 (20), 9136. http://dx.doi.org/10.1063/1.1567253. ISSN: 00219606 <http://scitation.aip.org/content/aip/journal/jcp/118/20/10.1063/1.1567253>.
Sun, H., 1998. COMPASS: an ab initio force-field optimized for condensed-phase applications overview with details on alkane and benzene compounds. J. Phys. Chem. B 102 (38), 7338–7364. http://dx.doi.org/10.1021/jp980939v. ISSN: 1520-6106 <http://pubs.acs.org/doi/abs/10.1021/jp980939v>.
Treutler, Oliver, Ahlrichs, Reinhart, 1995. Efficient molecular numerical integration schemes. J. Chem. Phys. 102 (1), 346. http://dx.doi.org/10.1063/1.469408. ISSN: 00219606 <http://scitation.aip.org/content/aip/journal/jcp/102/1/10.1063/1.469408>.
TURBOMOLE, 2014. TURBOMOLE V6.6. University of Karlsruhe and Forschungszentrum Karlsruhe GmbH. <http://www.turbomole.com>.
Wang, Moran, Pan, Ning, 2008. Modeling and prediction of the effective thermal conductivity of random open-cell porous foams. Int. J. Heat Mass Transfer 51 (5–6), 1325–1331. http://dx.doi.org/10.1016/j.ijheatmasstransfer.2007.11.031. ISSN: 00179310 <http://linkinghub.elsevier.com/retrieve/pii/S0017931007007028>.
Wassiljewa, A., 1904. Warmeleitung in Gasgemischen. Physikal. Z. 5 (22), 737–742.
Wells, Brad A., Chaffee, Alan L., 2015. Ewald summation for molecular simulations. J. Chem. Theory Comput. 11 (8), 3684–3695. http://dx.doi.org/10.1021/acs.jctc.5b00093. ISSN: 1549-9618 <http://pubs.acs.org/doi/abs/10.1021/acs.jctc.5b00093>.
Zhang, Meimei, Lussetti, Enrico, de Souza, Luis E.S., Miiller-Plathe, Florian, 2005. Thermal conductivities of molecular liquids by reverse nonequilibrium molecular dynamics. J. Phys. Chem. B 109 (31), 15060–15067. http://dx.doi.org/10.1021/jpO512255. ISSN: 1520-6106 <http://pubs.acs.org/doi/abs/10.1021/jpO512255>.